Periaxin is required for hexagonal geometry and membrane organization of mature lens fibers

Rupalatha Maddala[a], **Nikolai P. Skiba**[a], **Robert Lalane III**[a], **Diane L. Sherman**[b], **Peter J. Brophy**[b], and **Ponugoti V. Rao**[a,c,*]

[a]Department of Ophthalmology, Duke University School of Medicine, NC. USA

[b]Centre for Neuroregeneration, University of Edinburgh, Edinburgh, UK

[c]Department of Pharmacology and Cancer Biology, Duke University School of Medicine, NC. USA

Abstract

Transparency of the ocular lens depends on symmetric packing and membrane organization of highly elongated hexagonal fiber cells. These cells possess an extensive, well-ordered cortical cytoskeleton to maintain cell shape and to anchor membrane components. Periaxin (Prx), a PDZ domain protein involved in myelin sheath stabilization, is also a component of adhaerens plaques in lens fiber cells. Here we show that Prx is expressed in lens fibers and exhibits maturation dependent redistribution, clustering discretely at the tricellular junctions in mature fiber cells. Prx exists in a macromolecular complex with proteins involved in membrane organization including ankyrin-B, spectrin, NrCAM, filensin, ezrin and desmoyokin. Importantly, Prx knockout mouse lenses were found to be softer and more easily deformed than normal lenses, revealing disruptions in fiber cell hexagonal packing, membrane skeleton and membrane stability. These observations suggest a key role for Prx in maturation, packing, and membrane organization of lens fiber cells. Hence, there may be functional parallels between the roles of Prx in membrane stabilization of the myelin sheath and the lens fiber cell.

Keywords

Lens fibers; Cytoskeleton; Membrane organization; Periaxin; Schwann cells

Introduction

Periaxin (Prx) was first identified as a relatively abundant protein in myelinating Schwann cells during a screen for novel cytoskeletal-associated proteins with a role in peripheral nerve myelination (Gillespie et al., 1994). Prx has been thought to be expressed exclusively by myelinating Schwann cells (SCs) in a developmentally regulated manner (Gillespie et al., 1994; Scherer et al., 1995). In developing sciatic nerves, Prx is detected as the SCs ensheath axons, preceding proteins that characterize the myelin sheath (Scherer et al., 1995). Based

Correspondence to: P. Vasantha Rao, Ph.D, Department of Ophthalmology, Duke University School of Medicine, Durham, NC 27710, Phone: 919-681-5883; Fax: 919-684-8983, rao00011@mc.duke.edu.

on its localization to the Cajal bands of SCs (Court et al., 2004), and the demyelinating neuropathy phenotype associated with the gene knockout mouse model (Gillespie et al., 2000), Prx has been confirmed to play an essential role in stabilization of the SC-axon unit (Gillespie et al., 2000). Further, mutations in the human PRX gene cause autosomal recessive demyelinating Charcot-Marie-Tooth (CMT4F) disease (Boerkoel et al., 2001; Guilbot et al., 2001). Importantly, Prx has been shown to stabilize the dystroglycan glycoprotein complex (DGC) through direct interaction with the dystrophin-related protein 2 (DRP2) in a macromolecular complex that may provide a link between the extracellular matrix and the SC (Sherman et al., 2001).

While Prx expression was initially thought to be specific to myelinating SCs (Gillespie et al., 1994), it has since been reported in cytoskeletal complexes of lens fibers (Straub et al., 2003). Additionally, in the lens, Prx exists as part of the ezrin, periaxin, periplakin and desmoyokin (EPPD) complex, and is considered to play a role in cell adhesive interactions (Straub et al., 2003). Although the EPPD complex proteins are recognized to localize to the lens fiber cell plasma membrane (Straub et al., 2003), the functional significance of this protein complex, and the identity and nature of proteins that the EPPD complex interacts with to regulate fiber cell adhesion are not clear (Straub et al., 2003).

Lens architecture and transparency is dependent upon the unique cell shape, symmetric packing and membrane integrity of fiber cells, which comprise the bulk of the lens (Kuszak, 2004; Kuszak, 1996; Sandilands et al., 2003; Song et al., 2009; Yoon et al., 2008). These differentiated fiber cells are derived from epithelial cells that exit from the cell cycle at the equator and embark on a differentiation process that induces extensive cell elongation and membrane production (Lovicu and McAvoy, 2005; Piatigorsky, 1981), the loss of cellular organelles (Bassnett, 2002), reorganization of cytoskeleton and cell adhesive complexes (Bassnett et al., 1999; Bradley et al., 1980; Grey et al., 2009; Lee et al., 2000; Leong et al., 2000; Lo et al., 1997; Ramaekers et al., 1981; Song et al., 2009; Straub et al., 2003; Weber and Menko, 2006), and the expression of fiber-specific proteins including crystallins, aquaporin-0, connexins and beaded filaments (Ireland and Maisel, 1983; Piatigorsky, 1981). In cross-sectional profile, elongated lens fiber cells appear as flattened hexagons oriented along the lens circumference, which ensures the optimal packing of these cells necessary for lens transparency (Kuszak, 2004). Further, as organelle-free fiber cells become more closely packed, there is a marked elaboration of membrane interdigitations that are furrowed symmetrically in a ball and socket pattern (Blankenship et al., 2007; Kuszak, 2004; Willekens and Vrensen, 1982). While fiber cell hexagonal geometry and membrane organization including membrane interdigitations are considered critical determinants of lens optical clarity (Blankenship et al., 2007; Kuszak, 2004; Nowak et al., 2009; Sandilands et al., 2003; Song et al., 2009; Willekens and Vrensen, 1982; Yoon et al., 2008), the molecular and cellular bases of formation and maintenance of these structures are not well understood.

Here we report that Prx exhibits an intriguing expression profile relative to other EPPD complex proteins in normal eyes, localizing exclusively to lens fibers. Our study uncovers a crucial role for Prx in hexagonal geometry and membrane stabilization of mature lens fiber cells, likely through its membrane cytoskeletal scaffolding and domain organization activities.

Materials and methods

Mice

All the mice used in this study were from a C57BL/6 background. Embryonic day 10.5, 11.5, 12.5, 14.5 and neonatal (d1) eyes were used to assess developmental regulation of Prx

expression in the lens. Pregnant mice at specific gestational ages were sacrificed by pentobarbital injection, and fetuses removed by hysterectomy for tissue fixation of whole heads (Maddala et al., 2008). To obtain neonatal lenses, new born mice were sacrificed, whole eyes dissected out and incised at the posterior poles at the optic stalk, followed by immediate immersion in the respective fixative. Prx homozygous null mice were generated and characterized in the Brophy laboratory and genotyped as described earlier (Gillespie et al., 2000). These mouse lenses were confirmed to express BFSP2 which is known to be deleted in the mouse strain 129 (Sandilands et al., 2004). All animal procedures were conducted in accordance with the Duke University and University of Edinburgh institutional animal care guidelines and protocols.

Lens morphology by light and electron microscopy

Freshly enucleated eyes from postnatal (P24 and P90) Prx null and age-matched WT mice were fixed with 4% paraformaldehyde and 2.5% glutaraldehyde in 80 mM Na cacodylate buffer, pH 7.3, for 2 h at room temperature (RT), transferred to 2.5% glutaraldehyde, and stored in 10% buffered formalin at RT until further processing. The specimens were subsequently embedded in paraffin, and 5µm sections (equatorial plane) were cut and stained with hematoxylin and eosin. Micrographs were captured using Zeiss Axioplan2 microscopy (Zeiss Inc. Thornwood, NY. USA).

For transmission electron microscopy (TEM), buffered formalin (10%) fixed specimens were processed using a standard TEM protocol. Briefly, the tissue specimens were treated with 1% Osmium tetraoxide in 0.1 M Na cacodylate buffer, pH 7.2 at 4 °C for 1h. After rinsing with water and ethanol, the tissue specimens were treated with 2% uranyl acetate for 1 h at RT. Samples were then dehydrated through a series of ethanol grades (25% to 100%). Following this, the tissue sections were infiltrated with 1: 1 propylene oxide and spurr resin (SPI supplies), and exchanged with pure spurr and embedded at 65 °C overnight. Tissue specimens were cut (0.7 µ) in the equatorial plane using a Reichert Ultra-cut microtome (Leica), followed by ultra-thin sections (65 nm). Tissue sections were treated with 2% uranyl acetate and rinsed with 25% ethanol and water, and treated with 3.5% lead citrate. Images were captured at 8000x with a Jeol JEM-1400 equipped with Orius CCD digital camera at 60kV (JEOL, Tokyo, Japan).

Immunogold labeling

For aquaporin-0 immunogold labeling, freshly enucleated mouse eyes (P90 and P200) from both age-matched WT and Prx KO were first fixed in 10% buffered formalin at RT until further processing. The tissue specimens were labeled with immunogold by a standard protocol. Briefly, the formalin fixed lens tissue specimens were fixed with 0.125% glutaraldehyde containing 1% tanic acid in 0.1 M Na cacodylate buffer at RT. Then treated with 2% uranyl acetate for 1 h, followed by sequential dehydration using 50, 70, and 80% ethanol. Specimens were then embedded with pure LR White (55 °C, overnight). The embedded specimens were cut (65 nm) using a Leica ultra-microtome (Leica). Thin sections were blocked with PBS containing 10% goat serum and 0.1% Triton X-100 (blocking buffer). Specimens were incubated overnight at 4 °C with aquaporin-0 polyclonal antibody. Sections were rinsed with 2% goat serum in PBS, and then blocked again with blocking buffer at RT. Following this, sections were incubated with anti-rabbit IgG secondary antibody conjugated with gold (6 nm, Electron Microscopy Sciences) at RT for 2 h, then rinsed with PBS containing 2% goat serum. Specimens were then post fixed with 2% glutaraldehyde in 0.1 M Na cacodylate buffer, washed extensively with water, and treated with freshly prepared silver enhancement solution (HQ silver kit, Nanoprobes). The reaction was stopped by rinsing with water and the specimens were stained with 2% uranyl acetate,

followed with 3.5% lead citrate. Photographs were captured at 8000x with a Jeol JEM-1400 TEM equipped with Orius CCD digital camera.

Immunofluorescence analyses

For fluorescence immunostaining, eyes were fixed either for cryostat sectioning or paraffin sectioning. Cryostat sections (7 µm, sagittal plane) were obtained from embryonic heads (e10.5, e11.5, e12.5, e14.5) and neonatal eyes that were fixed in paraformaldehyde and sucrose until further processing (Maddala et al., 2008). The tissue sections were immunostained with polyclonal Prx antibody (Sigma-Aldrich) as we described earlier (Maddala et al., 2008) and images were captured with Nikon Eclipse 90i confocal laser scanning microscope (Nikon Instruments, Inc. Melville, NY. USA).

Immunofluorescence staining of paraffin embedded lens sections derived from Prx null and WT mice (P24, P90) were performed with specimens fixed in 10% formalin in PBS at RT. Five-micron tissue sections (equatorial plane) were de-paraffinized and rehydrated using xylene and absolute ethyl alcohol. Specimens were placed in the pre-heated antigen retrieval solution (0.1 M Na Citrate buffer pH 6.0) and heated with solution for 20 min at 100 °C. Then, the tissue sections were blocked for 10 min with the medical background Sniper reducing solution (Biocare Medical) in a humidified chamber. Primary antibodies were then applied (in 1% fatty acid free BSA in TBS), and incubated overnight at 4 °C in a humidified chamber. The following primary antibodies were used: NrCAM (polyclonal, Abcam), Prx (polyclonal, Sigma-Aldrich), aquaporin-0 (polyclonal, gift from Sam Zigler), β2-spectrin (monoclonal, BD Biosciences), Ankyrin B (monoclonal, gift from Vann Bennett), desmoyokin (monoclonal, Sigma-Aldrich), ezrin (monoclonal, Sigma-Aldrich), filensin (polyclonal, gift from Paul FitzGerald), N-cadherin (monoclonal, Invitrogen), β-catenin (monoclonal, Sigma-Aldrich), βIV-spectrin (polyclonal, gift from Masayuki Komada), contactin/F3 (monoclonal, Neuromab) and β-actin (monoclonal, Cell Signaling Technology). After incubation with primary antibodies, the slides were washed with TBS and incubated with either Alexa fluor 488 or 594 conjugated secondary antibodies (Invitrogen) in 1% BSA/TBS, for 2 h under dark conditions. Slides were rinsed with TBS and mounted using VectaMount and nail enamel, viewed and photographed using a Nikon Eclipse 90i confocal laser scanning microscope. For double-labeling, appropriate polyclonal and monoclonal antibodies were mixed and incubated with the tissue specimens as described above in conjunction with Alexa Fluor 488 and 594 conjugated second antibodies respectively (Invitrogen). For 3-D imaging (Fig. 2B, C (right panel), 2F (right panel)), images were acquired at RT using Zeiss LSM 510 inverted confocal microscope (Argon/2, 488; 561 nm Diode laser with motorized stage). Z Stacks (10 optical sections with step size 0.5 µm) with the 63×1.4 oil lens (Zeiss Plan Apochromat) were collected. Images were processed using Volocity 5.2.1 software and Adobe Photoshop.

Lens extracts

Membrane enriched fraction—Mouse lens membrane enriched fractions were isolated as we described earlier (Maddala et al., 2008) and the protein content was determined using the Bio-Rad protein assay reagent (Bio-Rad). Adult mouse sciatic nerve protein extract was prepared by homogenizing the nerves in hypotonic buffer (Rao et al., 2008) and the 800×g supernatant was used for immunoblot analysis.

Immunoprecipitations

To identify and characterize Prx interacting proteins in lens tissue, immunoprecipitation (IP) assays were performed using a Prx polyclonal antibody (Sigma-Aldrich), dynabeads protein G (Invitrogen), and Sigma-Aldrich IP buffer. Mouse lenses (pooled from the neonatal, P18 and adults) were homogenized (2% w/v) in $1 \times$ IP buffer containing protease inhibitors

(Roche protease inhibitor tablet, one/10 ml 1× IP buffer) and phosphatase inhibitors (Roche PhosStop tablet, one/10 ml 1× IP buffer) using a Dounce glass homogenizer on ice. Homogenates were centrifuged at 800×g for 10 min at 4 °C, and the supernatant was collected and protein content was measured using Bio-Rad reagent and used for IP reactions. IP reactions were performed by following the Invitrogen manufacturer protocol. The Prx immunocomplexes with dynabeads were separated from the sample and washed with PBST. Then 40 µl of 2X Lamelli sample buffer was added to the beads and boiled, and the protein samples were separated on the gradient SDS-PAGE (4–12%; Criterion XT precast gel from Bio-Rad) and stained with Gelcode® Blue stain reagent (Pierce). After destaining with Milli Q pure water, protein bands were excised from the gel and further characterized by mass spectrometry. Gel slices containing the protein bands were subjected to in-gel tryptic digestion using the In-Gel Tryptic digestion kit (Pierce), per manufacturer's instructions. This digestion process included both reduction and alkylation of protein samples.

Mass spectrometry

In-gel trypsin digested protein mixes were separated by reverse phase HPLC on the C18 capillary column and samples were analyzed on the MALDI-TOF-TOF 4700 Proteomic Analyzer (Applied Biosystems) using a selection of 10 precursors per spot in a mass range of 700–4000 Da and post-source decay for MS/MS acquisition as we described earlier (Maddala et al., 2007). Fragment peak lists were generated by *GPS* Explorer (Applied Biosystem Inc.) and searched against the NCBI Mouse database (May 2010 release) using mascot Server v2.2 with the following parameters: trypsin specificity allowing up to one missed cleavage, carbamidomethylation at Cys residues as fixed modification and protein N-termial acetylation and methionine oxidation as variable modifications. Precursor ion mass tolerance was set to 75 ppm and fragment mass tolerance was 0.5 Da. Precursors with masses corresponding to human keratin peptides were automatically excluded from the precursors lists generated by GPS after MS analysis. Acceptance criteria for protein identification required identification of at least two peptides for each protein with confidence interval percentage (CI%) over 99.90%, which corresponded to a false discovery rate of less than 1% in searching the NCBI mouse database.

Immunoblotting

To determine the changes in protein levels or detect the presence of given protein including Prx, ezrin, aquaporin 0, β-actin, β-spectrin, ankyrin B, NrCAM, and filensin in the immunoprecipitates or in the lens tissue or sciatic nerve fractions, equal volume of 2X Laemmli sample buffer was added and boiled for 5 min and were separated either on the gradient (4–12% or 4–15%) SDS-PAGE (Criterion, Bio-Rad) or on 12 or 8% SDS-PAGE casted gels, followed by electrophoretic transfer to nitrocellulose membrane (Bio-Rad) and immuno blots were developed as described earlier using appropriate polyclonal or monoclonal antibodies (Maddala et al., 2008). Immune positive bands were scanned using Fotodyne gel doc system, densitometrically quantified by imageJ software.

Quantifications

Fiber cell width—To measure the internal width of the fiber cells (Fig. 4E), 15 inch by 15 inch images (at 72 pixels/inch) are captured using Nikon Eclipse C90i confocal laser scanning confocal microscope with scale bar stamped on the image while capturing. These images with the 20µm scale bar are opened using the Photoshop software (Adobe Photoshop, version 7. 0.1), and using the "line tool", lines are drawn carefully inside the fiber cells, extending from one end of the inner wall to the other. Five cells are randomly picked (from the same regions of the Prx KO and WT lenses) from each image to measure the internal width, and "grid tool" is opened over the images, and using the 20µm scale bar

as reference, counted the number of grids on the lines as well as on the scale bar and calculated the width in µm. Equatorial sections (n=12) derived from four independent lenses from WT or Prx KO mice, stained either for β2-spectrin or aquaporin-0 are used to measure the internal width.

Membrane folds—For P90 (Fig. 7A) and P200 (Fig. 7B), two lens specimens from each group (WT and Prx KO) are processed for immuno EM as described above. From each specimen, images are captured starting from the epithelium, continuing into the regions of the lens outer cortical layers (OCL) and inner cortical layers (ICL) using a Joel JEM-1400 transmission electron microscope. Total number of membrane folding/beading per image is counted manually from both OCL and ICL regions.

Statistical analysis

Where required the Student's t-test was performed to determine significance of differences noted between the Prx KO and WT specimens using Sigma plot. Values are given as mean ± s.e.m.

Results

Periaxin exhibits lens preferred expression and developmental regulation in the eye

As evident from immunofluorescence analysis in Fig. 1A, Prx is localized primarily in lens fibers, with minimal detection in the lens epithelium, but is undetectable in the retina, cornea and other ocular tissues in mice. Given that Prx expression was previously thought to be specific to myelinating SCs (Gillespie et al., 1994), and that very little is known regarding its function in the lens (Straub et al., 2003), we sought to gain insight into the potential role of Prx in lens morphogenesis and function. To this end, we first evaluated the expression pattern of Prx in mouse eyes from embryonic day 10.5, 11.5, 12.5, 14.5 and neonatal (P1) eyes by immunofluorescence microscopy, using tissue cryosections (Fig. 1B). Prx expression is detectable as early as E10.5 in the lens pit with discrete distribution to the posterior region. During the different developmental stages evaluated, Prx expression is robustly induced in, and preferentially localized to fiber cells of the ocular lens (Fig. 1B). Moreover, Prx protein levels increased during lens maturation, as determined by immunoblot analysis of equal amounts of a lens membrane enriched protein fraction derived from P1, P7, P14, P21 and P60 mice (Fig.1C a). In the same samples, however, the levels of ezrin decrease gradually over the same time course (Fig. 1C b).

Periaxin exhibits maturation dependent redistribution and clustering at the vertices of mature lens fibers

The cellular distribution of Prx in lens fibers was probed using immunofluorescence confocal microscopy analysis of paraffin embedded P24 mouse lens equatorial sections (Fig. 2). Prx distributes to the fiber cell plasma membrane along both the long and short arms of the hexagonal fiber cells of the outer cortex, which represents the differentiating and maturing region within the growing lens. However, as fiber cells mature, Prx distribution was found to become prominent at the short arms of hexagonal fiber cells in the inner cortical region, exhibiting a discrete, plaque-like staining pattern at the tricellular junctions (vertices), and alternating with a much reduced staining at the bicellular junctions (between vertices, both short and long arms) as determined by both single plane (Fig. 2A) and 3-D (Fig. 2B) confocal imaging. This pattern is prominent in P18 and older lenses. The *en face* views of Prx distribution at the broad (Fig. 2B, left panel) and short (Fig. 2B, right panel) sides of fiber cells based on 3-D images reveal clustered distribution organized in a perfect braid at the short sides (arrows). Since the staining of Prx and other proteins analyzed in the

center (nucleus) of the lens was inconsistent due to the hardness of this region, our description is restricted to the cortical regions of the lens.

Additionally, Prx colocalizes with β-actin (Fig.2D) and exhibits partial colocalization with β-catenin (Fig. 2C, left: single plane, right: 3-D image) and N-cadherin (Fig. 2D) at the vertices of fiber cells as determined by confocal imaging. In contrast, at the long arms Prx was noted to colocalize with β-catenin and N-cadherin while β-actin was not detected in this region of mature fibers (Figs. 2C and D images represent the inner cortical lens region). In contrast to the codistribution of Prx and β-actin at vertices, filensin, a lens fiber specific intermediate filament protein (Ireland and Maisel, 1983; Merdes et al., 1991) required for lens architecture (Alizadeh et al., 2003), localizes to both the long and short arms of lens fibers, but displays a patch-like staining pattern at the center of the long arms of lens fibers (Fig. 2E, arrows). On the other hand, β2-spectrin, a major lens membrane skeleton protein (Lee et al., 2000), is localized to the fiber cell membrane in a pattern distinct from Prx, filensin and β-actin (Fig. 2F). β2-spectrin staining is detected throughout the short arm and approximately one-third the length of the long arm, but exhibits a much reduced staining intensity at the center of long arms (arrows) where filensin stains most strongly (Fig. 2E). At the vertices of the fiber cell, Prx colocalizes partially with β-spectrin (Fig. 2F, right panel: 3-D image). We conclude that this novel and unique spatial distribution of Prx, filensin, β-actin and β-spectrin to the tricellular and bicellular junctions of the prismoid lens fibers, as depicted in the schematic illustration in Figure 2G, is likely required for maintaining hexagonal shape and cell-cell interactions.

Evidence for Prx involvement in membrane cytoskeletal scaffolding

Since Prx is a known PDZ domain protein (Dytrych et al., 1998), we sought to explore whether Prx serves to mediate membrane scaffolding interactions in the lens by identifying Prx-interacting proteins in mouse lens tissue, using immunoprecipitation (IP) and mass spectrometry (MS) analyses (Fig. 3A). As compared to an IgG control, Prx antibody generated immunocomplexes contained several distinct proteins derived from the detergent suspended protein fraction (800×g supernatant) of whole mouse lenses (Fig. 3A). The Prx immunocomplexes were separated by gradient (4–12%) SDS-PAGE and subsequently identified by MALDI-TOF MS and MS/MS analyses. MS analysis identified several major protein constituents in the Prx immunocomplexes including, ankyrin B, spectrin (both α and β), plectin-1, Prx, desmoyokin, filensin, phakinin and vimentin (Fig. 3A). These results were confirmed in two independent experiments and the individual proteins were identified with high confidence (>99.5%) based on two or more peptides. While several minor constituents including aquaporin-0, connexin 50, synemin, lengsin, armadillo repeat gene related protein–ARVCF, catenin-α2, radixin, ezrin, actin, βb1-crystallin and microtubule-associated serine/threonine kinase (MAST) 2 and 4, were also detected in the Prx IPs, the identification of these proteins was based on either less than two peptides or with less than 99.5% confidence.

Immunoblot analysis of Prx immunocomplexes confirmed the presence of Prx, β-spectrin, Ankyrin B, NrCAM and filensin as shown in Fig. 3B. Ezrin was also confirmed to be present in the Prx immunocomplexes by Western blot (data not shown). Additionally, colocalization analysis revealed that Prx codistributes with desmoyokin and ezrin (Fig.3 C & D, respectively), and exhibits partial codistribution with Ankyrin B (Fig. 3E) at the vertices and long arms of fiber cells. In contrast to Prx (Fig. 2A), NrCAM was evenly distributed throughout the plasma membrane of fiber cells including both short and long arms (Fig. 3F).

Analysis of lens Prx immunocomplexes by gradient SDS-PAGE (4–12%) and MS consistently identified two distinct Prx proteins with molecular masses of ~160 kDa and ~180/190 kDa, with the latter being a prominent protein in the mouse lens (Fig. 3A). Both

protein bands exhibited strong immunoreactivity with Prx polyclonal antibody (Fig. 3B). The predominant form of Prx present in the lens migrates at higher molecular mass relative to sciatic nerve Prx as determined by immunoblot analysis (Fig. 3G). A similar Prx protein profile has been reported for bovine lens homogenates (Straub et al., 2003).

Disrupted lens fiber cell shape and packing in the Prx KO mouse model

To understand the role of Prx in lens fiber cell shape and packing, we performed histological characterization of Prx knockout (KO) mouse lenses by light and electron microscopy analyses. The adult Prx KO mice appear to develop eyes of normal size with no obvious phenotype based on direct visual examination. Further, freshly dissected Prx KO lenses derived from 6–9 month old mice were indistinguishable from age-matched wild type (WT) with respect to lens transparency, as assessed by light microscopy. Since these mice develop severe coordination defects after 6–9 months (Gillespie et al., 2000) and were euthanized after this period, the status of lens transparency in older Prx KO lenses is not known. However, to determine the changes in integrity of lens cytoarchitecture in the Prx KO mouse, eyes obtained from P24 and P90 Prx KO and age-matched WT mice were processed for light microscopy-based histology analysis. As expected, no Prx expression was evident by immunofluorescence analysis of the Prx KO lenses (Fig. 4A). Based on hematoxylin and eosin staining, no notable differences were evident at the levels of fiber cell organization, differentiation and migration between the Prx KO and WT lenses (Fig. 4B; data for P24 not shown).

However, during the tissue sectioning of these specimens for histological analysis, the Prx lenses were found to be softer than the respective age-matched WT lenses. Moreover, immunofluorescence staining of paraffin embedded lens equatorial sections obtained from the Prx KO and WT mice (P90) for membrane and membrane-associated proteins including β2-spectrin (Fig. 4C), aquaporin-0 (Fig. 4D), filensin and β-actin revealed notable abnormalities in fiber cell shape and arrangement, especially in the inner cortical regions (data for filensin and β-actin were identical to spectrin and aquaporin-0, not shown). Although the changes in fiber cell shape and arrangement are only subtle in the outer cortical fibers (OCF), the difference was much more pronounced in the inner cortical fibers (ICF) which undergo extensive membrane remodeling during terminal differentiation and compaction (Kuszak, 2004). These changes were much more pronounced in the P90 Prx KO lenses (Fig. 4) compared to the P24 lenses (R.L., unpublished). Fiber cells in affected areas (arrows) in the P90 Prx KO lenses were, on an average, significantly wider ($14.3 \pm 0.21 \mu m$, n = 44) than age and region-matched WT lens fiber cells ($6.4 \pm 0.47 \mu m$, n = 65; Fig. 4E). The lower panels in Fig. 4C and D show magnified areas (boxed) of inner cortical fibers from both WT and Prx KO lenses. Interestingly, this increase in fiber cell width did not impact all fiber cells uniformly and some fibers were smaller in width than WT (Fig.4 D, indicated with asterisks).

Evidence for disruption of membrane skeleton in Prx KO lenses

To explore whether the above described abnormalities of fiber cell shape and packing are associated with changes in levels of cytoskeletal and membrane proteins, we determined the levels of β2-spectrin, β-actin, filensin and aquaporin-0 in Prx KO lenses by immunoblotting analysis of soluble and membrane-rich protein fractions from P200 Prx KO and age-matched WT lenses. Since the lens defects associated with Prx KO mice show progression with increasing age, we used P200 lenses for these analyses. β2-Spectrin (73%), β-actin (70%) and aquaporin-0 (46%) protein levels were decreased significantly in the membrane-rich lens insoluble fraction of the Prx KO lenses compared to the WT lenses based on analysis of equal amounts of protein (Fig.5A & C). Filensin protein levels were elevated modestly (15%, Fig. 5C) in the membrane-rich insoluble fraction of the Prx KO mice.

Additionally, we compared the total protein profiles of membrane rich insoluble fractions from the P200 Prx KO and WT lenses by SDS-PAGE analysis and Coomassie blue staining. This analysis (Fig. 5B) revealed comparable protein profiles between the Prx KO and WT lenses, with the exception of an extra protein band at ~37kDa species (Fig. 5B, arrow) in the membrane- rich fraction of the Prx KO lenses. This extra protein band in the Prx KO lenses was found to be diffuse, implying that it could be a product of proteolytic degradation, which is a common characteristic of early lens opacification (Truscott et al., 1990). The 56 kDa Coomassie blue stained protein in fiber cell insoluble fractions in Fig. 5A indicates a loading control. Additionally, we examined for changes in the distribution pattern of desmoyokin and ezrin in the Prx KO lenses by immunofluorescence analysis, since these proteins co-immunoprecipitate with Prx from normal lenses. Both desmoyokin and ezrin exhibited a distorted distribution pattern in 90 day-old Prx KO mouse lenses, with reduced staining noted at the short arms of fiber cells relative to age-matched WT lenses (Fig. 5D, E).

Disrupted plasma membrane organization in Prx KO mouse lens fibers

Additional support for the above described morphological (Fig. 4) and cytoskeletal changes (Fig.5) in the Prx KO mouse lens fibers was obtained via transmission electron microscopy (TEM). The P90 Prx KO lenses (Fig. 6) exhibited abnormal fiber cell morphology with the fiber cell membrane exhibiting extensive membrane beading and folding, especially at the short arms compared to region-matched WT lens fibers (Fig. 6, arrows) which exhibit a symmetric fiber cell arrangement characterized by a typical hexagonal morphology. Further, as noted using confocal microscopy (Fig. 4C, D), lens fiber cell shape is altered in the Prx KO lenses, exhibiting increase in width and disruption of radial column organization (Fig.6). Membrane changes were prominent and pronounced in the fiber cells of the inner cortical region compared to the outer cortical fibers of the Prx KO lenses (Fig. 6, arrows). These conclusions were based on the data derived from 4 independent analyses.

Moreover, immunogold labeling of aquaporin-0 in the Prx KO lenses starting from the P90 stage (Fig. 7A) revealed a discontinuous membrane localization and clustering pattern compared to WT lens fibers which show a continuous distribution of aquaporin-0 along the plasma membrane (see the magnified inserts; Fig. 7). In both P90 and P200 Prx KO lenses (Fig. 7A & B, respectively), and consistent with previous observations (Figs.4 & 5), aquaporin-0 staining is reduced and clustered especially where the membrane is misfolded or beaded compared (Fig.7A & B, arrows) to corresponding regions of the WT lens. Further, we counted the number of membrane folds in both OCFs and ICFs and noted a significant increase in the ICFs of both P90 and P200 Prx KO lenses (Fig. 7C & D, respectively) compared to the WT lenses. Taken together, these multiple methods of analysis confirm impairment of fiber cell shape and membrane stability in the Prx KO lenses. Additionally, the Prx KO lens fiber cell specimens reveal a smooth cytoplasmic texture relative to a course texture in the WT lens fibers indicating certain subtle changes in the fiber cell cytoplasm due to absence of Prx (Fig.7).

Discussion

The hexagonal geometry, long-range ordered packing, and membrane organization of fiber cells are critical for optical clarity and deformability of the ocular lens. However, the structural and regulatory mechanisms driving the formation and stabilization of these characteristics of lens fibers are still unclear. Here we show that Prx, which is a PDZ domain protein involved in myelin sheath organization and stability (Dytrych et al., 1998; Gillespie et al., 2000; Sherman et al., 2001), is required for hexagonal geometries, packing and membrane stability of mature lens fiber cells. We made several significant observations in support of a role for Prx in these processes, including: preferential expression in lens tissue,

induction of expression during lens fiber cell differentiation, differentiation-dependent redistribution and discrete clustering to the vertices of fiber cells, and co-immunoprecipitation with proteins involved in cell adhesion and membrane organization. Most strikingly, the disruption of an ordered fiber cell arrangement, altered fiber cell shape and membrane perturbation in the Prx KO mouse lens, illuminate a vital role for Prx and Prx-containing macromolecular scaffolding complex consisting of ankyrin B, spectrin, NrCAM, ERM proteins, plectin 1, desmoyokin and filensin in maintenance of lens fiber cell hexagonal shape, ordered packing and membrane organization. Notably, although Prx expression starts early during lens development, the protein does not appear to be required for lens differentiation or growth. Prx is crucial, however, for maintenance of prismoid shape, mechanical properties and membrane stability of mature fiber cells more so than in maturing fiber cells, likely through its role in membrane cytoskeletal network connectivity, cell junctional stability, and scaffolding activity. These characteristics of Prx share some overlap the role(s) played by tropomodulin-1(Nowak et al., 2009), filensin (Blankenship et al., 2007), phakinin (Sandilands et al., 2003), ankyrin B (More et al., 2001) and NrCAM (More et al., 2001) in maintenance of lens cytoarchitecture.

Lens fiber cell hexagonal geometry and symmetric packing depends on cell adhesive interactions and cortical cytoskeletal protein organization (Leonard et al., 2010; Lo et al., 1997; Nowak et al., 2009; Straub et al., 2003). While the regulation of cell-cell interactions mediated by N-cadherin and β-catenin is well understood (Cain et al., 2008; Pontoriero et al., 2009), the formation and regulation of tricellular junctions of lens fibers is unclear (Leonard et al., 2008). This study reveals a unique distribution profile for Prx, wherein the protein is localized throughout the plasma membrane in maturing fiber cells in the lens outer cortex, but relocalizes predominantly to the vertices of the mature fiber cells (Fig.2) in the inner cortical region of lens which undergoes extensive cytoskeletal and membrane remodeling during terminal differentiation (Grey et al., 2009; Kuszak, 2004; Leonard et al., 2010; Song et al., 2009). Further, the dramatic changes observed in fiber cell width and arrangement in Prx KO lenses (Figs.4) provide evidence for the involvement of Prx in stabilization of fiber cell vertices and in the hexagonal geometry of this cell type. These changes are more pronounced in the ICFs than in the OCFs indicating a region preferred role for Prx within the lens. Although there is a general consensus regarding the mosaic distribution pattern between the EPPD complex proteins and N-cadherin/β-catenin in lens fibers (Straub et al., 2003), Prx is localized intensely to the vertices of the mature fiber cells with expression being specific to fiber cells (Fig.2A and B), suggesting that this protein might play a role of unique significance in lens cytoarchitecture. Additionally, the unique distribution profiles of different cytoskeletal proteins (filensin, spectrin, and actin) and of Prx along the fiber cell plasma membrane (Fig. 2) reflects the existence of discrete spatiotemporal cytoskeletal scaffolds which contribute to stabilizing the tricellular and bicellular junctions and the mechanical properties required for the hexagonal geometry and deformability of the unusually long and thin fiber cells (Fig.2G). Hence, it is plausible that the softer lenses, and fiber cell membrane instability and shape changes observed in the Prx KO mice (Figs.4–7) are indicative of impaired cell adhesive interactions and the mechanical properties that are regulated by Prx and Prx-associated scaffolding proteins (Fig.3). Intriguingly, while we see notable changes in fiber cell shape and arrangement, the adult Prx KO lenses appear to still be transparent. However, the refractive properties of these lenses may be impacted, as was noted for filensin (Alizadeh et al., 2003) and phakinin (Sandilands et al., 2003) null mice evaluated by laser scanning approaches. Further studies are needed to evaluate whether such changes also occur in the Prx KO lens.

The characteristics of Prx including its membrane localization (Fig. 2), accumulation in the cytoskeleton-enriched fraction (Gillespie et al., 1994; Straub et al., 2003), and presence of a PDZ domain at the N-terminus (Dytrych et al., 1998), indicate a potential role for Prx in

protein targeting/or macromolecular assembly at the cell cortical region. This conclusion is supported by the profile of lens proteins found to co-immunoprecipitate with Prx in our studies, including spectrin, ankyrinB, filensin, phakinin, desmoyokin, plectin-1, ERM proteins and NrCAM, along with aquaporin-0, connexin 50 and MAST 2 and 4, revealing a role for Prx in scaffolding of cytoskeletal network, cell junctional and signaling proteins. Ankyrin B and spectrin are well-characterized membrane scaffolding proteins (Bennett and Baines, 2001; Bennett and Healy, 2009). Spectrin and plectin-1 have previously been identified in EPPD complexes isolated from the bovine lens (Straub et al., 2003). However, we consistently identified the presence of ankyrin B, filensin, phakinin, NrCAM, along with aquaporin-0 and MAST kinases, in addition to spectrin and plectin, in Prx immunocomplexes from detergent suspended lens fractions (Fig.3). Although Prx immunocomplexes contained desmoyokin and ERM proteins, periplakin – which is a component of the EPPD complex (Straub et al., 2003), was not detected in this study which is consistent with a recent report by Yoon and Fitzgerald (Yoon and FitzGerald, 2009). However, it is also important to note that the IP protocols used in our study and in the Straub et. al (Straub et al., 2003) study are not identical. Interestingly however, phakinin, which was demonstrated to directly interact with periplakin (Yoon and FitzGerald, 2009), was one of the major components in Prx immunocomplexes characterized in this study (Fig.3). The fact that Prx could co-immunoprecipitate a vast array of cytoskeletal network components known to be engaged in macromolecular interactions with membrane proteins, together with other cell junctional and channel proteins described above, implies a role for Prx in membrane skeleton network connectivity, cell adhesive interactions, and membrane organization potentially through scaffolding activity. This scaffolding activity of Prx may be significant in both OCFs and ICFs as it is localized to the long and short arms of the OCF, in addition to its localization to the ICF. In SCs, Prx interacts with DRP2, a component of the DGC complex and in the absence of Prx, levels of DRP2 have been found to be depleted (Sherman et al., 2001). DRP2 was not found in the Prx ICs characterized in the current study although it was confirmed to be expressed in the lens tissue by RT-PCR analysis (Fig.S1).

It may be that the PDZ domain of Prx (Dytrych et al., 1998) and desmyoyokin (Komuro et al., 2004) participate in the macromolecule crowding noted in this study through either PDZ-PDZ domain interactions or through PDZ binding domains of interacting protein partners (Kim and Sheng, 2004). Absence of Dlg-1, a well characterized PDZ domain protein, impairs lens epithelial cell structure and fiber cell differentiation together with changes in aquaporin-0 protein levels (Rivera et al., 2009), confirming the importance of PDZ proteins in lens differentiation and membrane stability. Desmoyokin and Prx have been characterized as dual localization proteins (Salim et al., 2009; Straub et al., 2003). This is supported by the observation that desmoyokin distribution to the fiber cell membrane and vertices is markedly distorted in the absence of Prx (Fig.5E), indicating the importance of Prx and other EPPD complex proteins in stabilizing and organizing lens fiber cell membrane protein macromolecular complexes. Moreover, the instability of spectrin and actin noted in the Prx KO lenses (Fig. 5A) indicates that the membrane organization of these proteins and their stability is dependent on their interaction with the EPPD complex proteins and with ankyrin B, NrCAM and filensin. The organization of membrane-spanning proteins within discrete microdomains is critical for their physiological function (Bennett and Healy, 2009), and the cytoskeletal scaffolding networks contribute to the formation and maintenance of specialized membrane domains by anchoring networks of proteins that define the specific domain (Bennett and Healy, 2009; Fehon et al.; Ogawa et al., 2006; Salzer et al., 2008; Susuki and Rasband, 2008). The panoply of proteins found to co-immunoprecipitate with Prx in this study (Fig. 3) suggests that these proteins participate in membrane domain organization of lens fibers (Scheuring et al., 2007). Further, the extensive membrane perturbation (Figs. 6, 7), together with decreases in spectrin, actin and aquaporin 0 (Fig. 5) and clustering of aquaporion-0 noted in the Prx KO lenses (Fig.7) support a role for Prx in

fiber cell membrane organization and stability. Moreover, filensin, which was a major component in Prx immunocomplexes, has been shown to interact directly with aquaporin-0 through its C-terminus (Lindsey Rose et al., 2006), and to coexist with aquaporin 0 in broad side membrane invaginations of lens fiber cells (Grey et al., 2009). These characteristics of filensin also imply that this protein likely coordinates with Prx and other EPPD complex proteins to mediate fiber cell membrane stabilization and organization.

Importantly, ankyrin B, spectrin, NrCAM, ERM proteins, Prx and desmoyokin along with other neuronal abundant proteins including βIV-spectrin (Komada and Soriano, 2002; Yang et al., 2007), contactins (Gennarini et al., 1989; Peles et al., 1995; Sakurai et al., 1997), Caspr2 (Horresh et al., 2008; Poliak et al., 1999) and RPTPs (Bouyain and Watkins, 2010; Peles et al., 1995), which are expressed and distributed in lens fibers (Fig. S2) are demonstrated to play a crucial role in myelinating axons and to exist in clusters in membrane microdomains to stabilize ion channels at the axon initial segment and nodes of Ranvier (Bennett and Healy, 2009; Davis et al., 1996; Melendez-Vasquez et al., 2001; Peles et al., 1995; Poliak et al., 1999; Salim et al., 2009; Salzer et al., 2008; Sherman and Brophy, 2005; Susuki and Rasband, 2008). These similarities, together with the role of Prx and desmoyokin in membrane stabilization in myelinated SC (Gillespie et al., 2000; Salim et al., 2009) and lens fibers (Figs.5–7), raise the possibility for a distant analogy between lens fibers and myelinating SCs with respect to parallel mechanisms regulating cytoskeletal scaffolding required for membrane domain organization and stabilization. We speculate that there is a functional significance for the conserved membrane domain characteristics noted in the current study, to the regulation of channel protein activity in lens fibers. Prx and other EPPD complex proteins, acting in concert with ion channel stabilizing proteins described above (Figs. 3 and S2) may regulate ion channel activity and calcium homeostasis in addition to gap junction and water channel activity, thereby serving to control lens cytoarchitecture and mechanical properties.

Conclusions

This study reports that Prx is expressed in a lens specific manner within the eye and exhibits maturation dependent redistribution, localizing discretely at the vertices in mature lens fiber cells. Prx exists in a macromolecular complex with proteins involved in membrane organization including ankyrin-B, spectrin, NrCAM, filensin, ezrin and desmoyokin. Importantly, Prx knockout mouse lenses were found to be softer and more easily deformed than normal lenses, revealing disruptions in fiber cell hexagonal packing, membrane skeleton and membrane stability. These observations suggest a key role for Prx in maturation, packing, and membrane organization of lens fiber cells.

Highlights

- Peraiaxin, a PDZ domain protein involved in myelin sheath organization exhibits lens specific expression within the eye.

- Periaxin is developmentally regulated during lens differentiation, exhibits maturation dependent redistribution and localizes to the vertices in mature fiber cells.

- Periaxin exists in a macromolecular complex with proteins involved in membrane organization.

- Periaxin knockout mouse lenses reveal disruptions in fiber cell hexagonal packing, membrane skeleton and membrane stability.

> • Periaxin plays a key role in maturation, packing, and membrane organization of lens fiber cells.

Supplementary Material

Refer to Web version on PubMed Central for supplementary material.

Acknowledgments

References

Alizadeh A, Clark J, Seeberger T, Hess J, Blankenship T, FitzGerald PG. Targeted deletion of the lens fiber cell-specific intermediate filament protein filensin. Invest Ophthalmol Vis Sci. 2003; 44:5252–5258. [PubMed: 14638724]

Bassnett S. Lens organelle degradation. Exp Eye Res. 2002; 74:1–6. [PubMed: 11878813]

Bassnett S, Missey H, Vucemilo I. Molecular architecture of the lens fiber cell basal membrane complex. J Cell Sci. 1999; 112(Pt 13):2155–2165. [PubMed: 10362545]

Bennett V, Baines AJ. Spectrin and ankyrin-based pathways: metazoan inventions for integrating cells into tissues. Physiol Rev. 2001; 81:1353–1392. [PubMed: 11427698]

Bennett V, Healy J. Membrane domains based on ankyrin and spectrin associated with cell-cell interactions. Cold Spring Harb Perspect Biol. 2009; 1:a003012. [PubMed: 20457566]

Blankenship T, Bradshaw L, Shibata B, Fitzgerald P. Structural specializations emerging late in mouse lens fiber cell differentiation. Invest Ophthalmol Vis Sci. 2007; 48:3269–3276. [PubMed: 17591898]

Boerkoel CF, Takashima H, Stankiewicz P, Garcia CA, Leber SM, Rhee-Morris L, Lupski JR. Periaxin mutations cause recessive Dejerine-Sottas neuropathy. Am J Hum Genet. 2001; 68:325–333. [PubMed: 11133365]

Bouyain S, Watkins DJ. The protein tyrosine phosphatases PTPRZ and PTPRG bind to distinct members of the contactin family of neural recognition molecules. Proc Natl Acad Sci U S A. 2010; 107:2443–2448. [PubMed: 20133774]

Bradley RH, Lo WK, Kuszak J, Maisel H. The cytoskeleton of the chicken lens fiber cells: a scanning and ultrastructural analysis. Exp Eye Res. 1980; 31:487–494. [PubMed: 7449883]

Cain S, Martinez G, Kokkinos MI, Turner K, Richardson RJ, Abud HE, Huelsken J, Robinson ML, de Iongh RU. Differential requirement for beta-catenin in epithelial and fiber cells during lens development. Dev Biol. 2008; 321:420–433. [PubMed: 18652817]

Court FA, Sherman DL, Pratt T, Garry EM, Ribchester RR, Cottrell DF, Fleetwood-Walker SM, Brophy PJ. Restricted growth of Schwann cells lacking Cajal bands slows conduction in myelinated nerves. Nature. 2004; 431:191–195. [PubMed: 15356632]

Davis JQ, Lambert S, Bennett V. Molecular composition of the node of Ranvier: identification of ankyrin-binding cell adhesion molecules neurofascin (mucin+/third FNIII domain−) and NrCAM at nodal axon segments. J Cell Biol. 1996; 135:1355–1367. [PubMed: 8947556]

Dytrych L, Sherman DL, Gillespie CS, Brophy PJ. Two PDZ domain proteins encoded by the murine periaxin gene are the result of alternative intron retention and are differentially targeted in Schwann cells. J Biol Chem. 1998; 273:5794–5800. [PubMed: 9488714]

Fehon RG, McClatchey AI, Bretscher A. Organizing the cell cortex: the role of ERM proteins. Nat Rev Mol Cell Biol. 11:276–287. [PubMed: 20308985]

Gennarini G, Cibelli G, Rougon G, Mattei MG, Goridis C. The mouse neuronal cell surface protein F3: a phosphatidylinositol-anchored member of the immunoglobulin superfamily related to chicken contactin. J Cell Biol. 1989; 109:775–788. [PubMed: 2474555]

Gillespie CS, Sherman DL, Blair GE, Brophy PJ. Periaxin, a novel protein of myelinating Schwann cells with a possible role in axonal ensheathment. Neuron. 1994; 12:497–508. [PubMed: 8155317]

Gillespie CS, Sherman DL, Fleetwood-Walker SM, Cottrell DF, Tait S, Garry EM, Wallace VC, Ure J, Griffiths IR, Smith A, Brophy PJ. Peripheral demyelination and neuropathic pain behavior in periaxin-deficient mice. Neuron. 2000; 26:523–531. [PubMed: 10839370]

Grey AC, Li L, Jacobs MD, Schey KL, Donaldson PJ. Differentiation-dependent modification and subcellular distribution of aquaporin-0 suggests multiple functional roles in the rat lens. Differentiation. 2009; 77:70–83. [PubMed: 19281766]

Guilbot A, Williams A, Ravise N, Verny C, Brice A, Sherman DL, Brophy PJ, LeGuern E, Delague V, Bareil C, Megarbane A, Claustres M. A mutation in periaxin is responsible for CMT4F, an autosomal recessive form of Charcot-Marie-Tooth disease. Hum Mol Genet. 2001; 10:415–421. [PubMed: 11157804]

Horresh I, Poliak S, Grant S, Bredt D, Rasband MN, Peles E. Multiple molecular interactions determine the clustering of Caspr2 and Kv1 channels in myelinated axons. J Neurosci. 2008; 28:14213–14222. [PubMed: 19109503]

Ireland M, Maisel H. Identification of native actin filaments in chick lens fiber cells. Exp Eye Res. 1983; 36:531–536. [PubMed: 6343103]

Kim E, Sheng M. PDZ domain proteins of synapses. Nat Rev Neurosci. 2004; 5:771–781. [PubMed: 15378037]

Komada M, Soriano P. [Beta]IV-spectrin regulates sodium channel clustering through ankyrin-G at axon initial segments and nodes of Ranvier. J Cell Biol. 2002; 156:337–348. [PubMed: 11807096]

Komuro A, Masuda Y, Kobayashi K, Babbitt R, Gunel M, Flavell RA, Marchesi VT. The AHNAKs are a class of giant propeller-like proteins that associate with calcium channel proteins of cardiomyocytes and other cells. Proc Natl Acad Sci U S A. 2004; 101:4053–4058. [PubMed: 15007166]

Kuszak, JR.; Costello, MJ. The structure of the vertebrate lens. In: Lovicu, FJ.; Robinson, ML., editors. Development of the Ocular lens. Cambridge: Cambridge Univ Press; 2004. p. 71-118.

Kuszak JR, Zoltoski KL, Brown G. Electron microscopic observations of the crystalline lens. Mocrosc. Res. Tech. 1996; 33:441–479.

Lee A, Fischer RS, Fowler VM. Stabilization and remodeling of the membrane skeleton during lens fiber cell differentiation and maturation. Dev Dyn. 2000; 217:257–270. [PubMed: 10741420]

Leonard M, Chan Y, Menko AS. Identification of a novel intermediate filament-linked N-cadherin/gamma-catenin complex involved in the establishment of the cytoarchitecture of differentiated lens fiber cells. Dev Biol. 2008; 319:298–308. [PubMed: 18514185]

Leonard M, Zhang L, Zhai N, Cader A, Chan Y, Nowak RB, Fowler VM, Menko AS. Modulation of N-cadherin junctions and their role as epicenters of differentiation-specific actin regulation in the developing lens. Dev Biol. 2010

Leong L, Menko AS, Grunwald GB. Differential expression of N- and B-cadherin during lens development. Invest Ophthalmol Vis Sci. 2000; 41:3503–3510. [PubMed: 11006245]

Lindsey Rose KM, Gourdie RG, Prescott AR, Quinlan RA, Crouch RK, Schey KL. The C terminus of lens aquaporin 0 interacts with the cytoskeletal proteins filensin and CP49. Invest Ophthalmol Vis Sci. 2006; 47:1562–1570. [PubMed: 16565393]

Lo WK, Shaw AP, Wen XJ. Actin filament bundles in cortical fiber cells of the rat lens. Exp Eye Res. 1997; 65:691–701. [PubMed: 9367649]

Lovicu FJ, McAvoy JW. Growth factor regulation of lens development. Dev Biol. 2005; 280:1–14. [PubMed: 15766743]

Maddala R, Reneker LW, Pendurthi B, Rao PV. Rho GDP dissociation inhibitor-mediated disruption of Rho GTPase activity impairs lens fiber cell migration, elongation and survival. Dev Biol. 2008; 315:217–231. [PubMed: 18234179]

Maddala R, Skiba N, Vasantha Rao P. Lens fiber cell elongation and differentiation is associated with a robust increase in myosin light chain phosphorylation in the developing mouse. Differentiation. 2007; 75:713–725. [PubMed: 17459090]

Melendez-Vasquez CV, Rios JC, Zanazzi G, Lambert S, Bretscher A, Salzer JL. Nodes of Ranvier form in association with ezrin-radixin-moesin (ERM)-positive Schwann cell processes. Proc Natl Acad Sci U S A. 2001; 98:1235–1240. [PubMed: 11158623]

Merdes A, Brunkener M, Horstmann H, Georgatos SD. Filensin: a new vimentin-binding, polymerization-competent, and membrane-associated protein of the lens fiber cell. J Cell Biol. 1991; 115:397–410. [PubMed: 1918147]

More MI, Kirsch FP, Rathjen FG. Targeted ablation of NrCAM or ankyrin-B results in disorganized lens fibers leading to cataract formation. J Cell Biol. 2001; 154:187–196. [PubMed: 11449000]

Nowak RB, Fischer RS, Zoltoski RK, Kuszak JR, Fowler VM. Tropomodulin1 is required for membrane skeleton organization and hexagonal geometry of fiber cells in the mouse lens. J Cell Biol. 2009; 186:915–928. [PubMed: 19752024]

Ogawa Y, Schafer DP, Horresh I, Bar V, Hales K, Yang Y, Susuki K, Peles E, Stankewich MC, Rasband MN. Spectrins and ankyrinB constitute a specialized paranodal cytoskeleton. J Neurosci. 2006; 26:5230–5239. [PubMed: 16687515]

Peles E, Nativ M, Campbell PL, Sakurai T, Martinez R, Lev S, Clary DO, Schilling J, Barnea G, Plowman GD, Grumet M, Schlessinger J. The carbonic anhydrase domain of receptor tyrosine phosphatase beta is a functional ligand for the axonal cell recognition molecule contactin. Cell. 1995; 82:251–260. [PubMed: 7628014]

Piatigorsky J. Lens differentiation in vertebrates. A review of cellular and molecular features. Differentiation. 1981; 19:134–153. [PubMed: 7030840]

Poliak S, Gollan L, Martinez R, Custer A, Einheber S, Salzer JL, Trimmer JS, Shrager P, Peles E. Caspr2, a new member of the neurexin superfamily, is localized at the juxtaparanodes of myelinated axons and associates with K+ channels. Neuron. 1999; 24:1037–1047. [PubMed: 10624965]

Pontoriero GF, Smith AN, Miller LA, Radice GL, West-Mays JA, Lang RA. Co-operative roles for E-cadherin and N-cadherin during lens vesicle separation and lens epithelial cell survival. Dev Biol. 2009; 326:403–417. [PubMed: 18996109]

Ramaekers FC, Boomkens TR, Bloemendal H. Cytoskeletal and contractile structures in bovine lens cell differentiation. Exp Cell Res. 1981; 135:454–461. [PubMed: 7308306]

Rao PV, Ho T, Skiba NP, Maddala R. Characterization of lens fiber cell triton insoluble fraction reveals ERM (ezrin, radixin, moesin) proteins as major cytoskeletal-associated proteins. Biochem Biophys Res Commun. 2008; 368:508–514. [PubMed: 18261459]

Rivera C, Yamben IF, Shatadal S, Waldof M, Robinson ML, Griep AE. Cell-autonomous requirements for Dlg-1 for lens epithelial cell structure and fiber cell morphogenesis. Dev Dyn. 2009; 238:2292–2308. [PubMed: 19623611]

Sakurai T, Lustig M, Nativ M, Hemperly JJ, Schlessinger J, Peles E, Grumet M. Induction of neurite outgrowth through contactin and Nr-CAM by extracellular regions of glial receptor tyrosine phosphatase beta. J Cell Biol. 1997; 136:907–918. [PubMed: 9049255]

Salim C, Boxberg YV, Alterio J, Fereol S, Nothias F. The giant protein AHNAK involved in morphogenesis and laminin substrate adhesion of myelinating Schwann cells. Glia. 2009; 57:535–549. [PubMed: 18837049]

Salzer JL, Brophy PJ, Peles E. Molecular domains of myelinated axons in the peripheral nervous system. Glia. 2008; 56:1532–1540. [PubMed: 18803321]

Sandilands A, Prescott AR, Wegener A, Zoltoski RK, Hutcheson AM, Masaki S, Kuszak JR, Quinlan RA. Knockout of the intermediate filament protein CP49 destabilises the lens fibre cell cytoskeleton and decreases lens optical quality, but does not induce cataract. Exp Eye Res. 2003; 76:385–391. [PubMed: 12573667]

Sandilands A, Wang X, Hutcheson AM, James J, Prescott AR, Wegener A, Pekny M, Gong X, Quinlan RA. Bfsp2 mutation found in mouse 129 strains causes the loss of CP49 and induces vimentin-dependent changes in the lens fibre cell cytoskeleton. Exp Eye Res. 2004; 78:109–123. [PubMed: 14667833]

Scherer SS, Xu YT, Bannerman PG, Sherman DL, Brophy PJ. Periaxin expression in myelinating Schwann cells: modulation by axon-glial interactions and polarized localization during development. Development. 1995; 121:4265–4273. [PubMed: 8575326]

Scheuring S, Buzhynskyy N, Jaroslawski S, Goncalves RP, Hite RK, Walz T. Structural models of the supramolecular organization of AQP0 and connexons in junctional microdomains. J Struct Biol. 2007; 160:385–394. [PubMed: 17869130]

Sherman DL, Brophy PJ. Mechanisms of axon ensheathment and myelin growth. Nat Rev Neurosci. 2005; 6:683–690. [PubMed: 16136172]

Sherman DL, Fabrizi C, Gillespie CS, Brophy PJ. Specific disruption of a schwann cell dystrophin-related protein complex in a demyelinating neuropathy. Neuron. 2001; 30:677–687. [PubMed: 11430802]

Song S, Landsbury A, Dahm R, Liu Y, Zhang Q, Quinlan RA. Functions of the intermediate filament cytoskeleton in the eye lens. J Clin Invest. 2009; 119:1837–1848. [PubMed: 19587458]

Straub BK, Boda J, Kuhn C, Schnoelzer M, Korf U, Kempf T, Spring H, Hatzfeld M, Franke WW. A novel cell-cell junction system: the cortex adhaerens mosaic of lens fiber cells. J Cell Sci. 2003; 116:4985–4995. [PubMed: 14625392]

Susuki K, Rasband MN. Molecular mechanisms of node of Ranvier formation. Curr Opin Cell Biol. 2008; 20:616–623. [PubMed: 18929652]

Truscott RJ, Marcantonio JM, Tomlinson J, Duncan G. Calcium-induced opacification and proteolysis in the intact rat lens. Invest Ophthalmol Vis Sci. 1990; 31:2405–2411. [PubMed: 2173688]

Weber GF, Menko AS. Actin filament organization regulates the induction of lens cell differentiation and survival. Dev Biol. 2006; 295:714–729. [PubMed: 16678812]

Willekens B, Vrensen G. The three-dimensional organization of lens fibers in the rhesus monkey. Graefes Arch Clin Exp Ophthalmol. 1982; 219:112–120. [PubMed: 7173625]

Yang Y, Ogawa Y, Hedstrom KL, Rasband MN. betaIV spectrin is recruited to axon initial segments and nodes of Ranvier by ankyrinG. J Cell Biol. 2007; 176:509–519. [PubMed: 17283186]

Yoon KH, Blankenship T, Shibata B, Fitzgerald PG. Resisting the effects of aging: a function for the fiber cell beaded filament. Invest Ophthalmol Vis Sci. 2008; 49:1030–1036. [PubMed: 18326727]

Yoon KH, FitzGerald PG. Periplakin interactions with lens intermediate and beaded filaments. Invest Ophthalmol Vis Sci. 2009; 50:1283–1289. [PubMed: 19029034]
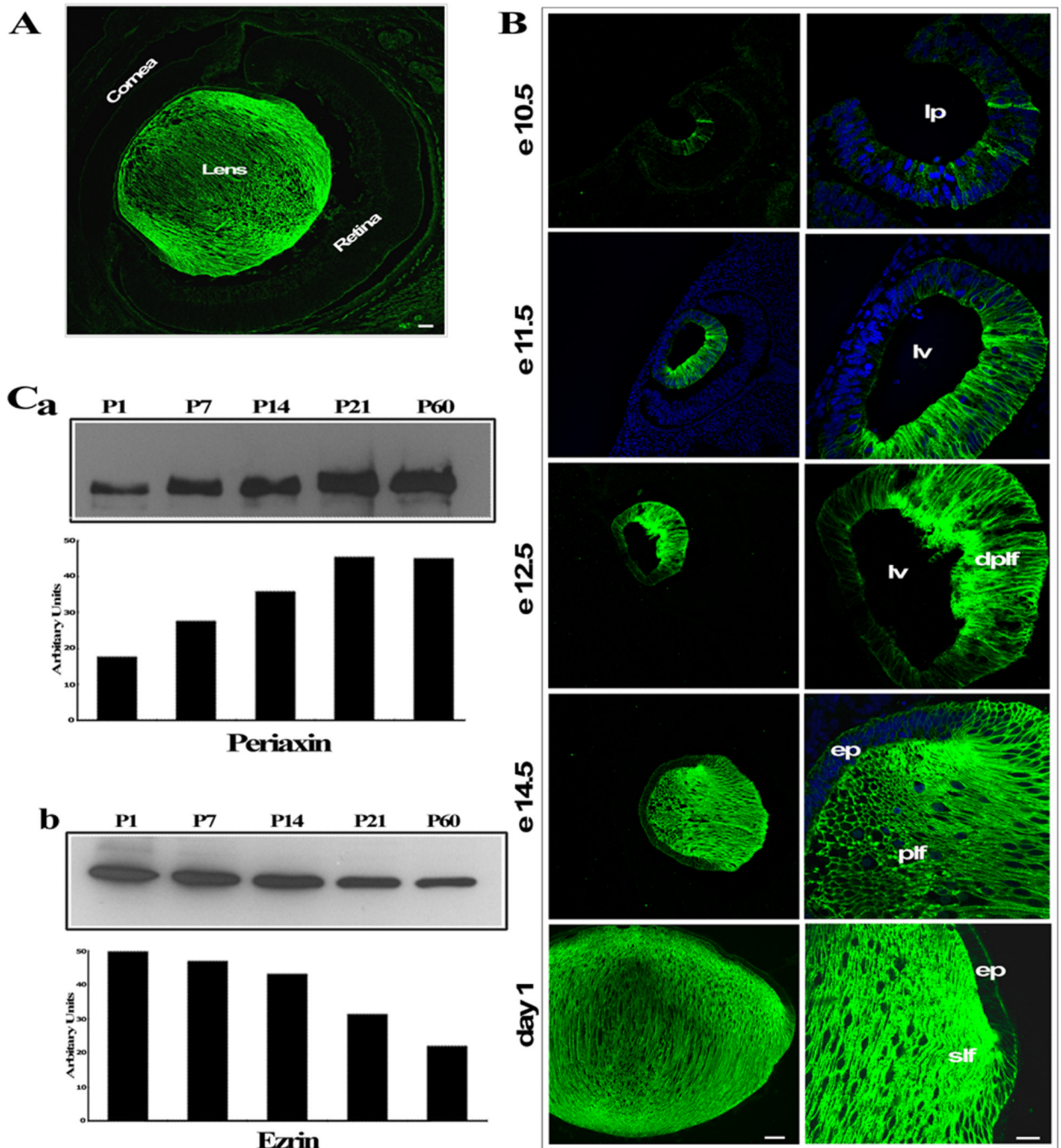
Figure 1.
Periaxin exhibits preferential expression in ocular lens fibers and robust induction during lens morphogenesis. (A) Immunofluorescence (green) analysis of the embryonic (E14.5) mouse eye (sagittal plane) reveals preferential distribution of Prx in lens tissue within the developing eye. (B) Analysis of developmental regulation by immunofluorescence staining of e10.5, e11.5, e12.5, e14.5 and day-1 specimens reveals Prx expression starting in the posterior lens pit (lp) and lens vesicle (lv), with a robust induction in the differentiating primary lens fibers (dplf), and distributing primarily to the primary (plf) and secondary (slf) lens fibers with barely detectable staining of the lens epithelium (ep). The blue stain shows cell nuclei labeled with DAPI. (C a) Prx protein levels assessed in P1, P7, P14, P21 and P60

mouse lenses by Western blot, reveals a gradual increase from P1 to P21 then reaching a plateau by P60 based on densitometric analysis (histograms). (C b) In the same samples, however, protein levels of ezrin decrease gradually over the same time course. Bars: (A) 40μm; (B) left panel: 100μm, right panel: 20μm.
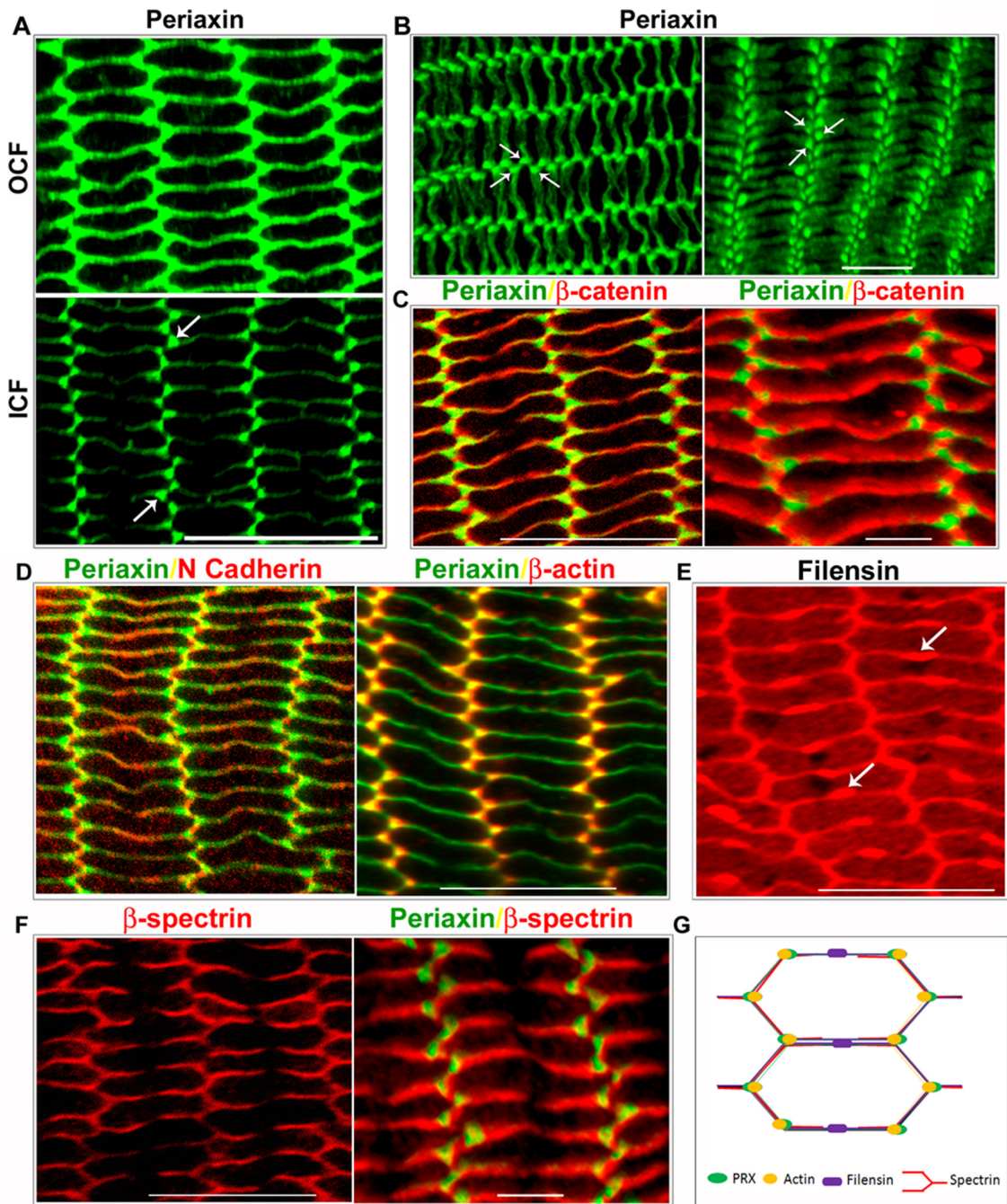
Figure 2.
Periaxin exhibits maturation dependent redistribution in mouse lens fibers with an intense plaque-like accumulation at the vertices of the mature fiber cells. (A) Equatorial paraffin sections of P24 mouse lens stained for Prx, and representative confocal microscope images are shown for the outer cortical (OCF) and inner cortical fibers (ICF) with Prx localizing throughout the cell membrane in OCF and mostly to the vertices in the ICF (arrows); (B) 3-D images of Z stacks of Prx staining from the ICFs of mouse lens, *en face* views of broad (left) and short (right) sides; (C) Single plane (left panel) and 3-D (right panel) images of Z stacks of lens equatorial sections (from the inner cortical region) stained for Prx and β-catenin showing a mosaic distribution pattern between Prx and β-catenin at fiber cell short

arms; (D) Equatorial sections of P24 mouse lens double stained for Prx and N-cadherin or β-actin. Merged images (single plane) reveal a mosaic distribution pattern between Prx and N-cadherin at fiber cell short arms (images were derived from the inner cortical region of lens). Relative to N-cadherin, β-actin shows a complete colocalization with Prx at the vertices; (E) Filensin distribution in P24 mouse lenses; filensin is distributed throughout the fiber cell membrane with a patch-like accumulation localized discretely at the center of long arms (arrows); (F) β2-spectrin distribution in P24 mouse lenses; (left panel) β2-spectrin is nearly undetectable at the center of the long arms (arrows) but exhibits a continuous staining to the short arm and extending to the 1/3 of the long arm resulting in a horse shoe shape pattern; (right panel) 3-D images of Z stacks of lens equatorial sections stained for Prx and β2-spectrin. (G) Schematic illustration of spatial distribution of Prx, β-actin, filensin and β2-spectrin in the hexagonal lens fiber cell. Bars: (A) 20 µm, (B) 10 µm, (C) left and right 20 and 10 µm, respectively, (D) 20 µm, (E) 20 µm, (F) left and right 20 and 10 µm, respectively.
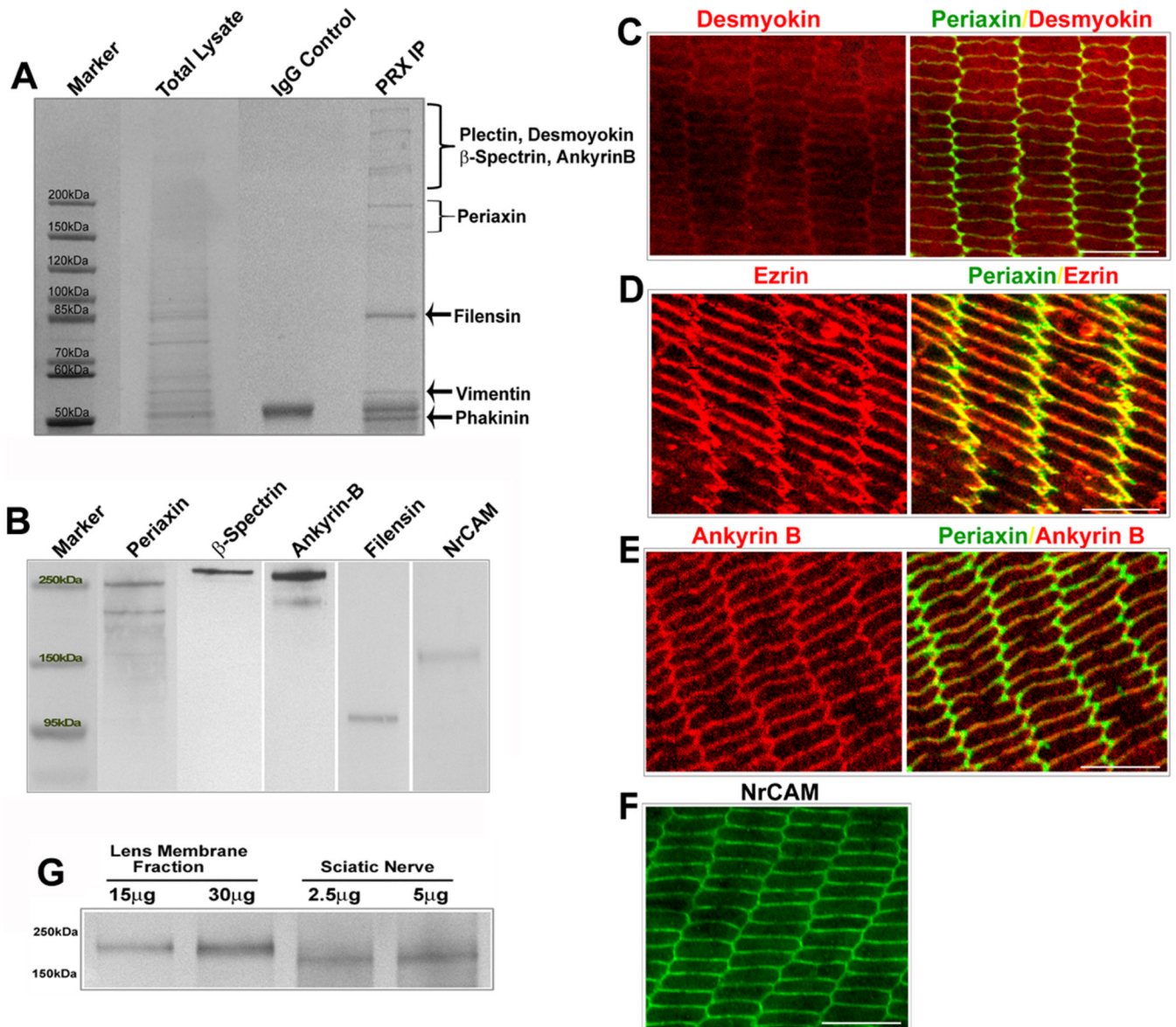
Figure 3.
Scaffolding interactions of Prx as evidenced by coimmunoprecipitation analysis, MALDI-MS, and immunoblotting. (A) Gelcode blue stained, gradient SDS-PAGE (4–12% polyacrylamide) separation of protein complexes immunoprecipitated from the mouse lens homogenates using a Prx antibody, annotated with MALDI-MS identification (labeled on the right side of figure). (B) Immunoblot-based identification of individual proteins from Prx immunocomplexes generated from the mouse lens homogenates. (C, D, E) Equatorial paraffin sections of P24 mouse lens double stained for Prx and desmoyokin, ezrin or ankyrin B or (F) stained for NrCAM alone. Representative confocal microscope images are shown. (G). Comparison of Prx profile between the mouse lens and sciatic nerve by immunoblotting. Relative to sciatic nerve Prx, lens Prx migrates at a slightly higher molecular mass. Bars: (C, D, E and F) 20 µm.
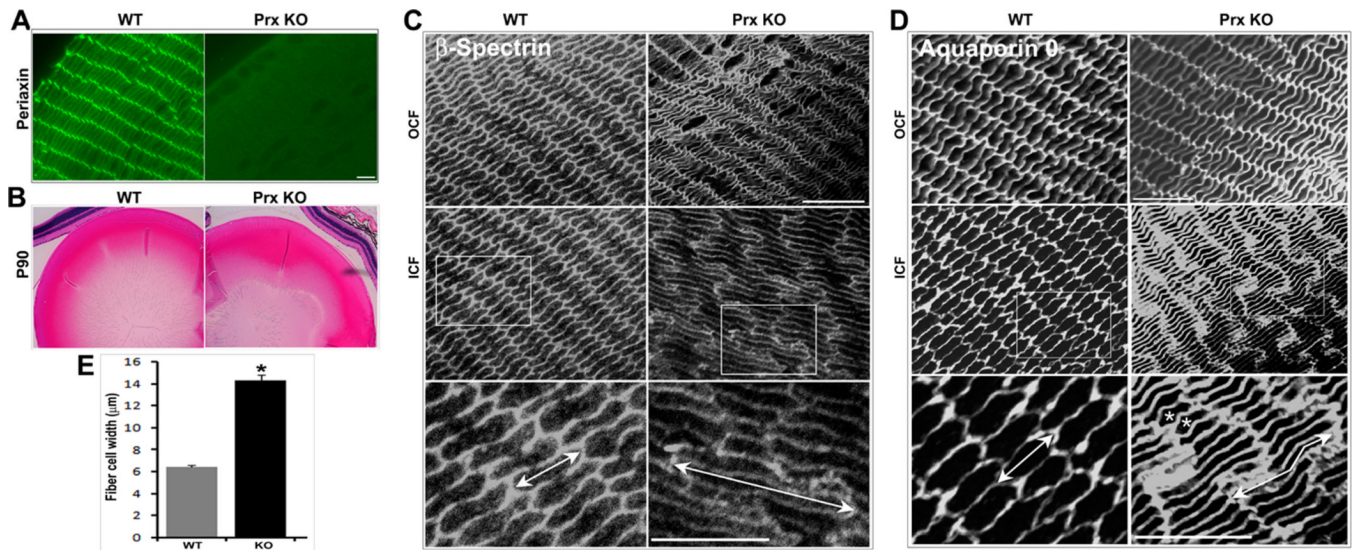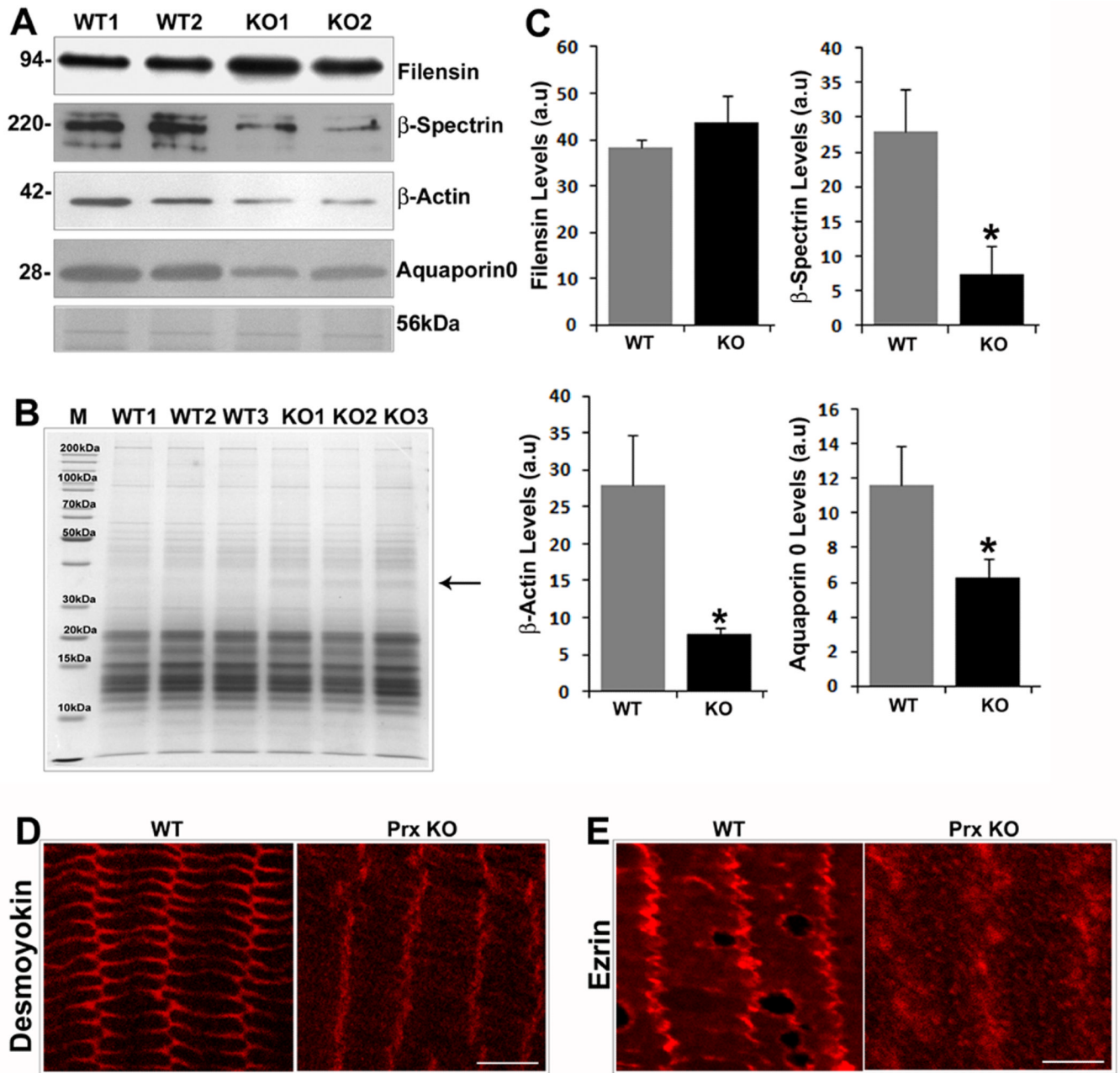
Figure 4.
Hexagonal geometry and radial column organization of lens fiber cells is disrupted in the absence of Prx. (A) Equatorial paraffin lens sections derived from P90 Prx KO and age-matched WT mice assessed for Prx distribution (green) by immunofluorescence; (B) Light microscope-based histological analysis of P90 lenses with hematoxylin and eosin staining; (C & D) Equatorial sections of P90 lenses from Prx KO and WT mice, respectively, stained for β2-spectrin and aquaporin-0; Higher magnification (2.5×) of boxed area is shown in the bottom panels; (E) In some subpopulations of fiber cells, cell width from Prx KO lenses is increased significantly ($p<0.001$) compared to the corresponding fiber cells from WT lenses. In contrast, some Prx KO lens fibers exhibited reduced width as indicated by asterisks. Cell width (arrows) was measured from the tissue sections derived from four independent lenses. OCF: Outer cortical fibers; ICF: Inner cortical fibers. Bars: (C & D) 10μm.

Figure 5.
Membrane protein profiles are altered in lenses lacking Prx. (A, C) Immunoblot analysis and quantification of membrane-rich fraction derived from the P200 Prx KO and age-matched WT mouse lenses showed significant decreases (* P<0.001) in the levels of β2-spectrin, β-actin and aquaporin-0 in the absence of Prx; filensin levels are modestly (15%) elevated in the Prx KO lenses. The Coomassie blue stained 56 kDa protein in the lens membrane rich fraction represents a loading control; (B) SDS-PAGE (12.5%), followed by Coomassie blue staining of the lens membrane rich protein fraction (10 µg) derived from the Prx KO and WT mice shows an additional distinct band at ≈37 kDa (arrow) in all three samples (2–4 lenses were pooled per sample) of Prx KO lenses. a.u: arbitrary units. (D, E) Immunofluorescence analysis of desmoyokin and ezrin in P90 Prx KO and age-matched WT

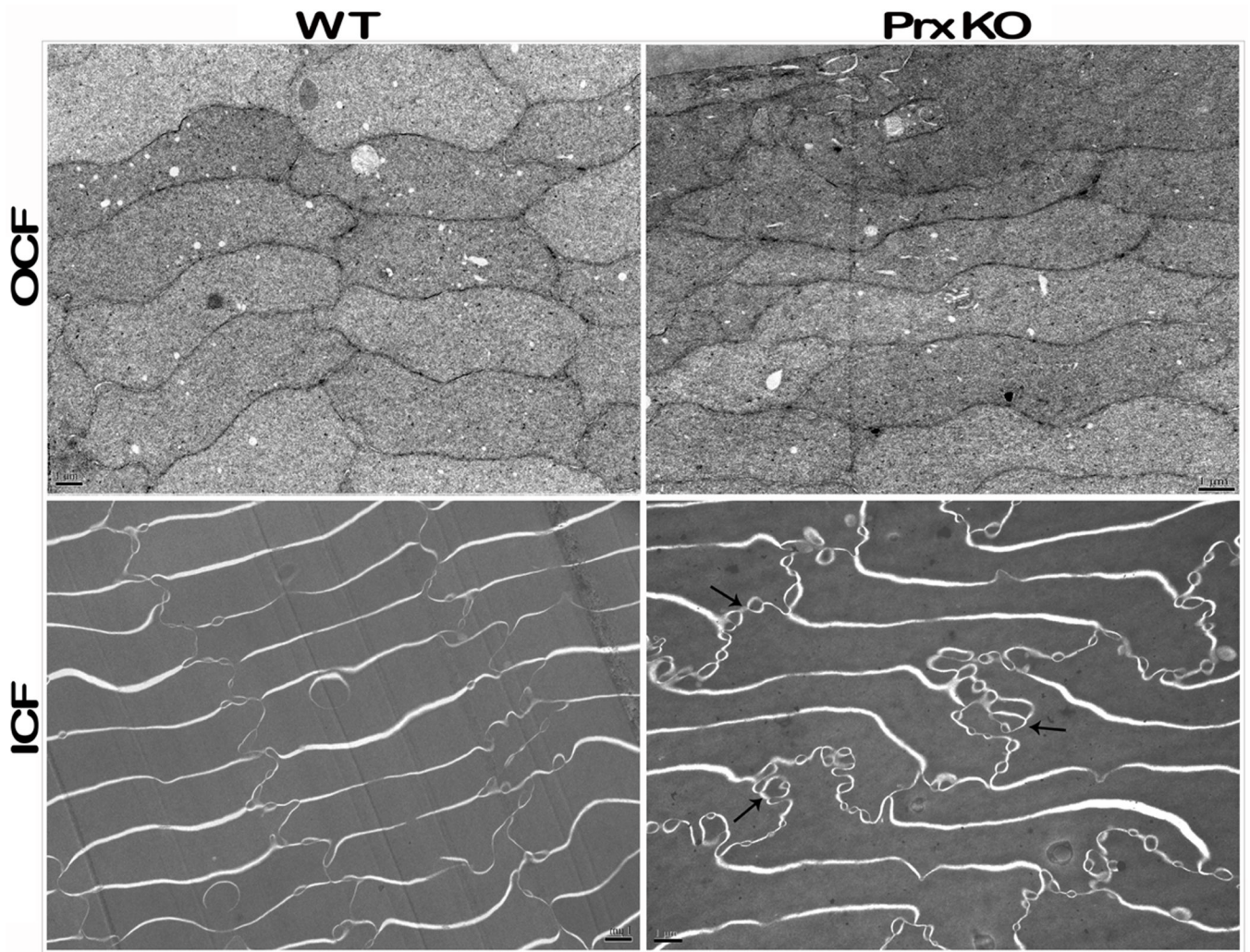lenses revealed disruption in their organization at the fiber cell short arms in the Prx KO mice. Bars: (D, E) 20 µm.

Figure 6.
Lens fiber cells exhibit extensive membrane beading and folding with altered shape in the absence of Prx as demonstrated by TEM-based histology. Representative TEM images of P90 lens fibers from the outer cortical (OCF) regions and inner cortical (ICF) regions of Prx KO and WT mouse lenses, showing extensive membrane folding/beading (arrows) associated with misalignment in fiber cell organization and changes in cell shape. Bar:1µm.
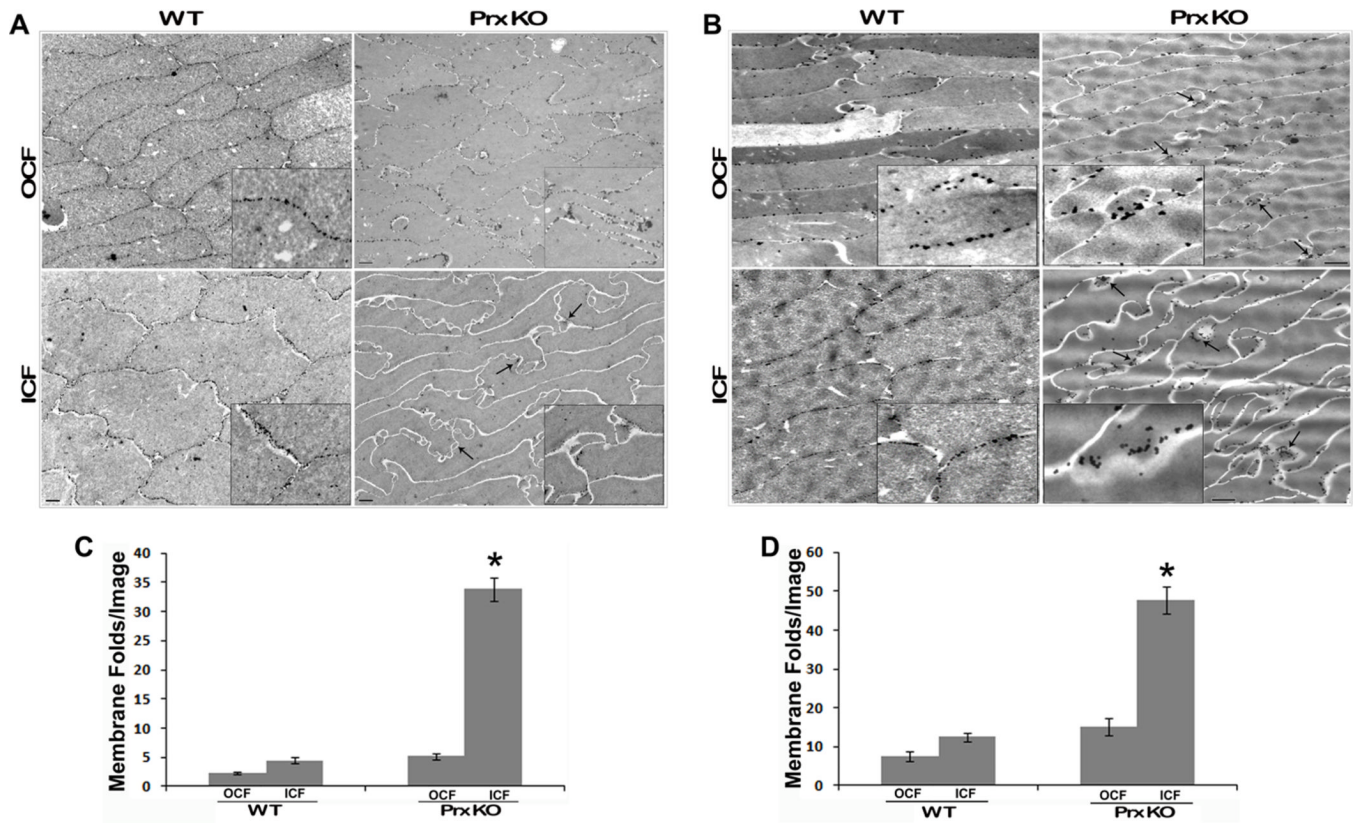
Figure 7.
Periaxin absence leads to discontinuous and clustered organization of Aquaporin-0 in the lens fiber cell membrane in association with increased membrane misfolding as demonstrated by immunogold labelling. Representative images of immunogold distribution pattern of aquaporin-0 in lens fiber cells from the outer and inner cortical regions of P90 (A) and P200 (B) Prx KO and age-matched WT mice. Inserts show higher magnification (2.5×) of the image. (C & D) Significant (P<0.001) increase in membrane folds/beading are observed in Prx KO lens fibers compared to the respective WT fiber cells. Bars: (A & B) 1µm.